International Journal of Engineering, Mathematical and Physical Sciences
ISSN: 2517-9934
Vol:7, No:8, 2013

Onset Velocity Profiles Evolution in Microchannels

Cătălin Mărculescu, Andrei Avram, Cătălin Pârvulescu, Marioara Avram, and Cătălin Mihai Bălan

***Abstract*—**The present microfluidic study is emphasizing the flow behavior within a Y shape micro-bifurcation in two similar flow configurations. We report here a numerical and experimental investigation on the velocity profiles evolution and secondary flows, manifested at different Reynolds numbers (*Re*) and for two different boundary conditions. The experiments are performed using special designed setup based on optical microscopic devices. With this setup, direct visualizations and quantitative measurements of the path-lines are obtained. A Micro-PIV measurement system is used to obtain velocity profiles distributions in a spatial evolution in the main flows domains. The experimental data is compared with numerical simulations performed with commercial computational code FLUENT in a 3D geometry with the same dimensions as the experimental one. The numerical flow patterns are found to be in good agreement with the experimental manifestations.

***Keywords*—**Micro-PIV, numerical investigations, secondary flows, velocity profiles.

I. Introduction

IT is an intuitive fact that microfluidics, as an emerging application in applied fluid mechanics, is dealing with methods and devices that control and manipulate fluids with the length scale on the order of micrometer [1]. Beside their small size which is an extremely important character of microfluidic devices, the low cost and fast analyses are other two important characteristics of these devices. The laminar flows, short molecular diffusion distances and the capability for high control and manipulation of flows are also fundamental but less obvious characteristics [2].

In this paper, our focus is to emphasize the velocity profiles evolution in a Y-microbifurcation, for two distinct situations in which the initial boundary conditions are slightly different. Another objective is focused on the manifestation and evolution of secondary flows for the same Newtonian flows (test fluid is deionized water). The Y bifurcation is used in the present experiments with the setup of two inlets and one outlet. In one situation the boundary condition involves two inlets and one outlet respectively. In the second situation one of the inlets is maintained blocked for all experiments.

These investigations are performed with a direct understanding of the microfluidic behavior in one of the most common flow configurations, Y-bifurcation.

The test geometries used in the present application are an in house made silicon microfluidic chips covered with a glass slide, and are in the shape of an Y-bifurcation with the cross-section of 300μm x 300 μm (Fig. 1 (g), with two ore one inlet (Fig. 3 (c) and (d)).

The numerical results were compared with anextensive experimental investigation. The experimental measurements were performed on a special set-up made ofan optical inverted microscope and a CCD camera connected on the microscope's objective. Using this setup, direct visualizations and quantitative measurements for the two case studies are obtained. The quantitative experimental method that was employed to characterize the performance of our microfluidic device was the particle image velocimetry (PIV) method for velocity measurements at micrometer scale. Micro-resolution PIV refers to the measurement technique wherein fluid motion is measured in a spatially resolved manner with the length scale ranging from 10^{-4} to $10^{-7}m$ [3].To make the motion of the fluid observable, tracer particles are added within the bulk flow. Two images of the moving particles are then captured and analyzed using spatial correlation methods that calculate the fluid velocity fields from the motion of the tracer particles over an know time interval, Δt.

II. Experimental Methodology

A. Device Fabrication

The microchannels were fabricated in silicon wafers (100 *mm* – 4 in. diameter, 525-550 μm thick, Semiconductors Wafer, Inc. Hsinchu, Taiwan) with deep reactive ion etching technology (ICP-RIE - Oxford Plasmalab System 100) using the Bosch process (Fig. 1 (a)-(e)). The characteristic parameters for plasma process were: *Passivation step:* flow rate C4F8 100 sccm; ICP power 700 *W*; RF power 10 *W*; pressure 20 *mT*; time 5 *s*; *Etching step:* flow rate SF6 100 *sccm*; ICP power 700 *W*; RF power 25 *W*; pressure 20 *mT*; time 7 *s* (general parameters: He back-pressure was 10 *T*, electrode temperature 15° C and etching rate ~ 2.8 $\mu m \cdot min^{-1}$).

The microfluidic test section must be designed with at least one optically transparent wall, so that it can be viewed with the objective lens of the inverted microscope employed in the experimental investigations.

C. M. Bălan is with the National Institute for R&D in Microtechnologies IMT-Bucharest, *Micro and Nano Fluidics Laboratory*, Bucharest, 077190, Romania (corresponding author phone: 004 0723 195 649; fax: 021-269 07 72; e-mail: catalin.balan@imt.ro).

C. Mărculescu, A. Avram, C. Pârvulescu and M. Avramare also with the National Institute for R&D in Microtechnologies IMT-Bucharest, *Micro and Nano Fluidics Laboratory*, Bucharest, 077190, Romania (e-mails: catalin.marculescu@imt.ro; andrei.avram@imt.ro; catalin.parvulescu@imt.ro; marioara.avram@imt.ro).

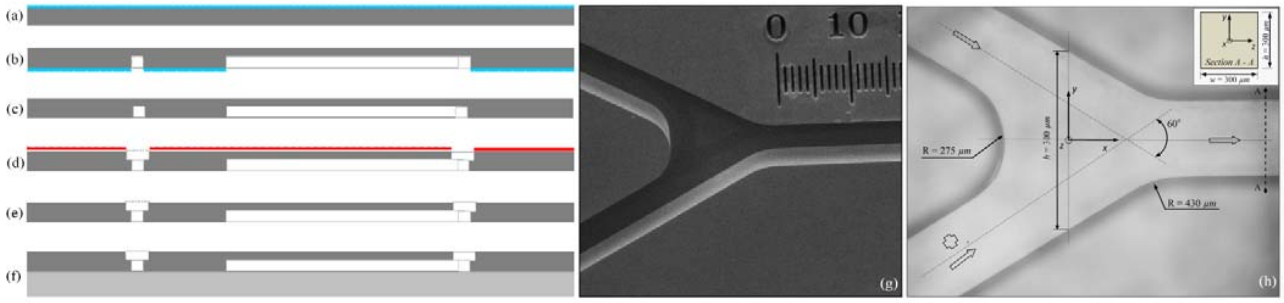

Fig. 1 Main steps of the fabrication process of the silicon chip: (a) growth of a SiO_2 layer; (b) pattering the SiO_2 layer and the 1st deep RIE process; (c) removing the oxide mask; (d) the 2nd deep RIE process through a photoresist mask; (e) removing the photoresist mask; (f) anodic bonding of the silicon chip to a borosilicate glass wafer. (g) SEM picture of the bifurcation zone (one division from scale represents 50 μm) and (h) optical image of the bifurcation with geometrical characteristics and the position of the coordinate system (x = y = z = 0)

Due to this reason the silicon wafers have been sealed by anodic bonding with a borosilicate glass wafer (100 *mm* diameter, 0.7 *mm* thick, Pyrex 7740 – Fig. 1 (f)). Fluidic access through-holes with 1 *mm* in diameter were also etched by DRIE at each microchannel terminus. On one silicon wafer, six different microfluidic devices were fabricated, each having the same general configuration and depth (of 300 μm), and with the widths of the microchannels of 300 μm. After the DRIE processes the silicon wafers were anodically bonded (400° C and a bonding voltage of 1000 *V*) to glass wafers to seal the microchannels.

Polytetrafluoroethylene (PTFE) tubing was attached to the fluidic access points using commercially available fluidic ports (Idex Health & Science GmbH, Wertheim, Germany). The fluidic nanoports were bonded on the backside of the silicon wafers with adhesive rings delivered by the supplier at a temperature of 165° for one hour. PTFE capillary tubes (Idex Health & Science GmbH, Wertheim, Germany) with an inner diameter of 0.5 *mm* connected the fluidic ports with the remote chambers (Remote Chamber 400, Dolomite, Charlestown, MA) that contain the test fluids, deionized water seeded with fluorescent microspheres with a diameter of 0.9 μm(Duke Scientific Corporation, Fremont, CA, USA). A constant and pulseless fluid flow was maintained with a precise pressure driven pumping mechanism (Mitos P-Pump, Dolomite, Charlestown, MA) connected to the laboratory compressed air port, and controlled via computer with a dedicated software (developed within the acknowledged project, in an LabView interface).

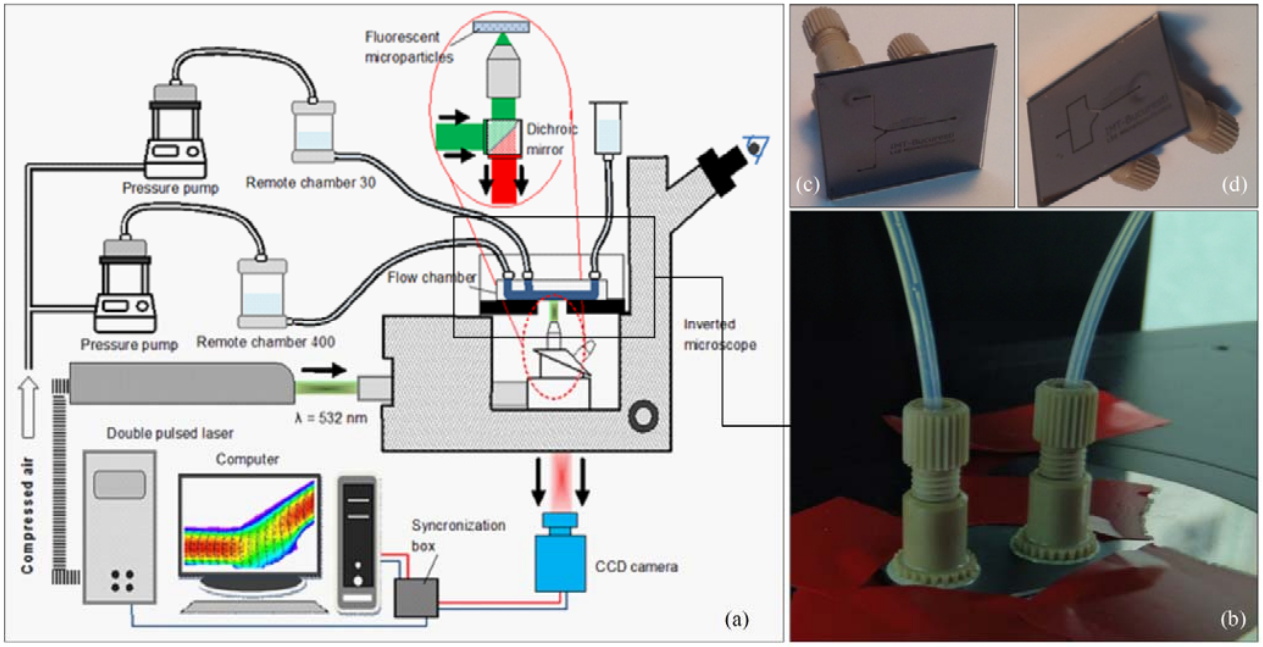

Fig. 2 (a) Micro-PIV set-up with the schematic optical path (detail of the filter cube); (b) setup connections of the microfluidic chips; (c) Microfluidic chip with two inlets but with one fluidic path maintained closed and; (d) microfluidic chip with one fluidic path but with both Y branches maintained open

B. Micro-PIV Measurements and Visualizations

A schematic drawing of the used epifluorescent Micro-PIV system is presented in Fig. 2 (a). The system performs invasive velocity measurements and hydrodynamic characterization of the microfluidic flows. A double-pulsed laser is used to generate monochromatic Nd: YAG laser light (NewWave Research, Fremont, CA). These types of laser systems are specifically designed for PIV application [3] and consist of two Nd: YAG laser cavities, beam-combining optics, and frequency-doubling crystals (Dualpower 30-15, 2 x 30 mJ 15 Hz). The laser emits two light pulses at a wave length of $\lambda = 532$ *nm*. The pulse duration is of the order of 10 *ns*, and the time delay between light pulses can vary from tens of nanoseconds to a few seconds. The illumination light is delivered to the inverted microscope to illuminate the microfluidic device. The optical connection between the microscope and the laser is maintained by an optical fiber cord.

A barrier filter must be positioned between the mirror and the relay lens (represented in detail in Fig. 2) that passes the fluorescent light from the seed particles, while filtering out illumination light that is reflected by the surface of the test section [3]. A dichroic mirror (Fig. 2 (a) – detail) is used to perform the separation of illumination light from the emitted fluorescent light of the fluorescently labeled seed particles. The light spots are recorded by a CCD camera (charge-couple device) with two sensors and in a large-format array 2048 x 2048 (Dantec HiSense 4M) in a large spatial dynamic range.

In volume illumination, the entire depth of the test section is illuminated by a volumetric cone of light [4], and the measurements plane must be defined by the depth-of-field of the recording lens. Microscopic objective lens, 10X, used present large apertures, NA = 0.22, with sharply defined objective planes, thereby allowing particles to transition quickly from being in focus to being in out of focus. Following the equation presented by Meinhart et al. [5] and Olsen & Adrian [6] describing the measurement depth for volume illumination, the measurements corresponds to $\delta_{zm} \approx 76\ \mu m$ (for 10X, with NA = 0.22) deep-of-field, which represents up to 25% of the channel height. For all cases, a minimum of 70 image pairs were recorded and divided into interrogation areas of 32 x 32 pixels. These images were processed and averaged ensemble using the software package ImageManager (version 4.71) delivered by Dantec. In the image post-processing technic a Nyquist algorithm with a 50% overlap was used in generate the 2D velocity profiles maps.

III. Analytical Consideration and Simulations

A. Governing Equations

For an incompressible fluid flow, the governing equations for mass conservation and momentum can be expressed as follows:

$$\nabla \cdot \mathbf{v} = 0 \tag{1}$$

$$\rho\left[\frac{\partial \mathbf{v}}{\partial t} + (\mathbf{v}\nabla)\mathbf{v}\right] = \rho\mathbf{b} - \nabla p + 2\nabla(\eta(\dot{\gamma})\mathbf{D}) \tag{2}$$

where ρ is the fluid density (assumed constant), **b** is the unitary mass force, **D** is the stretching, **v** the velocity vector, p the pressure andthe viscosity function, dependent on shear rate (for a Newtonian fluid= constant – present cases).

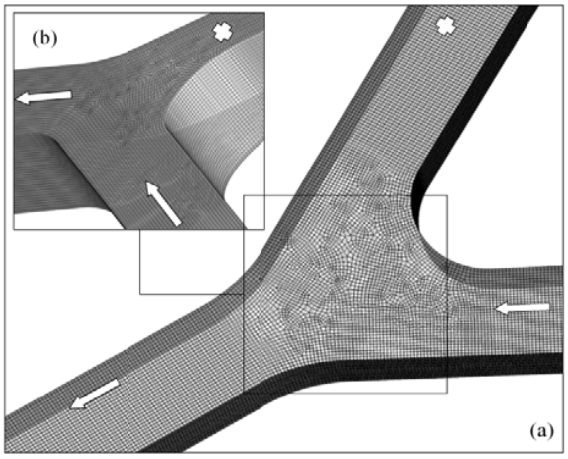

Fig. 3 (a) Close up view of the virtual mesh with a (b) detail near the bifurcation area

The validity of the continuum hypothesis and the no-slip boundary condition were assumed also for all studied cases. The flow domain has been discretized using a structured mesh containing 1 043 370 hexahedral finite elements (Fig. 3). For the investigated cases a 3D model with pressure based solver, implicit and steady flow scheme was used. The computed solution presents a precision of 10^{-10}.

B. Dimensionless Numbers

1. Reynolds Number

Even if the microfluidic flows are laminar by nature, the Reynolds number (*Re*), which describes the relative importance of inertial forces to viscous forces, is still one of the most important dimensionless numbers. Control volume analysis of fully developed flow in microchannel leads to the concept of a hydraulic radius described in terms of the flow area (A) and wetted perimeter (P): $R_h = A/P$ [7].

This quantity provides a simple way of characterizing a channel of non-circular cross-section using a single characteristic length scale. In microfluidics, where is common to deal with channels of planar cross-section, it is typical to define *Re* as a function of the hydraulic radius $R_h = h \cdot w/2(h+w)$ and the average velocity ($V = Q/h \cdot w$, where Q represents the volumetric flow rate, and h respectively w are the characteristic dimensions of the microchannel cross-section – Fig. 1 (h), resulting in:

$$Re = \frac{4\rho V R_h}{\eta_0}, \tag{3}$$

where ρ is fluid density ($kg \cdot m^{-3}$), and η_0 is the dynamic viscosity ($Pa \cdot s$).

2. Dean Number

Because of the deviations in the geometry design, and with the increase of flow rate, a type of secondary flows will manifest. These are the Dean vortices that are manifesting especially in elbows [8] and curved channels [9], [10]. These secondary flows will have, in our case studied, a direct impact on the velocity profiles shape from the main flow domain.

The magnitude of these secondary flows can be quantified by another dimensionless number named Dean number (De), and expressed as:

$$De = \frac{4\rho V R_h}{\eta_0}\sqrt{\frac{4R_h}{R}} = Re\sqrt{4\frac{R_h}{R}}, \quad (4)$$

where R is the radius of curvature of the channel path ($R = 600$ μm). It is obvious that for a straight microchannel, $De = 0$, indicating the absence of Dean flows. In a curved microchannel, on the other hand, De increases with higher curvature (smaller R), larger channel size (larger R_h), and with the increase of the flow rate (higher Re) [9], [10].

IV. Results and Discussions

The numerical results were compared to the experimental investigation, consisting of direct visualizations and quantitative observations. The results are in good agreement, considering the approximations of the numerical model, in order to reduce the total convergence time. Also the direct visualizations with the Micro-PIV system are not performed in a single median plane, but in a series of very close planes with a spread of a few microns. This led to some small differences compared to the numerical predictions.

A. Measurement Validation on the Case with One Branch Closed

The first case in which the experimental measurements and numerical predictions are validated is the flow configuration with one branch maintained closed. The Micro-PIV measurements were conducted in both the open and closed branch, in the region indicated on the Fig. 4 (b) (section A-A). By the experimental and the numerical evaluation two effects were observable in the manifestation of the microfluidic flow with the increase of the inertia ($Re \rightarrow \infty$).

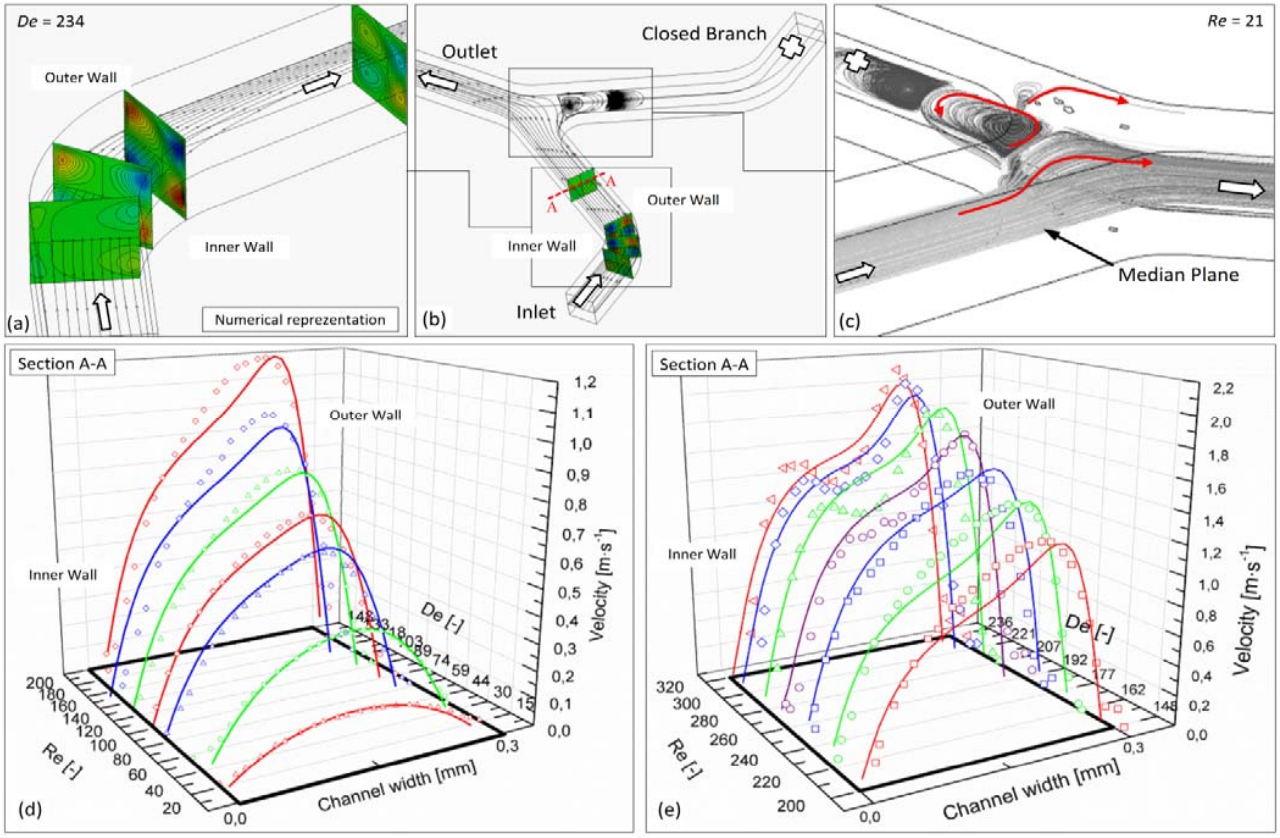

Fig. 4 Numerical predictions of the microfluidic flow with an emphasis of the 3D character the flow. Manifestations of the secondary flows as (a) Dean vortices (representation of the Vz component; $De = 234$) and (c) spiral vortex that communicate with primary flow from the open branch, $Re = 21$; (b) The virtual geometry on which the simulations were performed.(d) - (e) Comparison of experimental velocity distribution (open symbols – micro-PIV measurements), with numerical predictions (continues lines) obtained for a single phase (deionized water) at different flow regimes ($20 < Re < 320$)

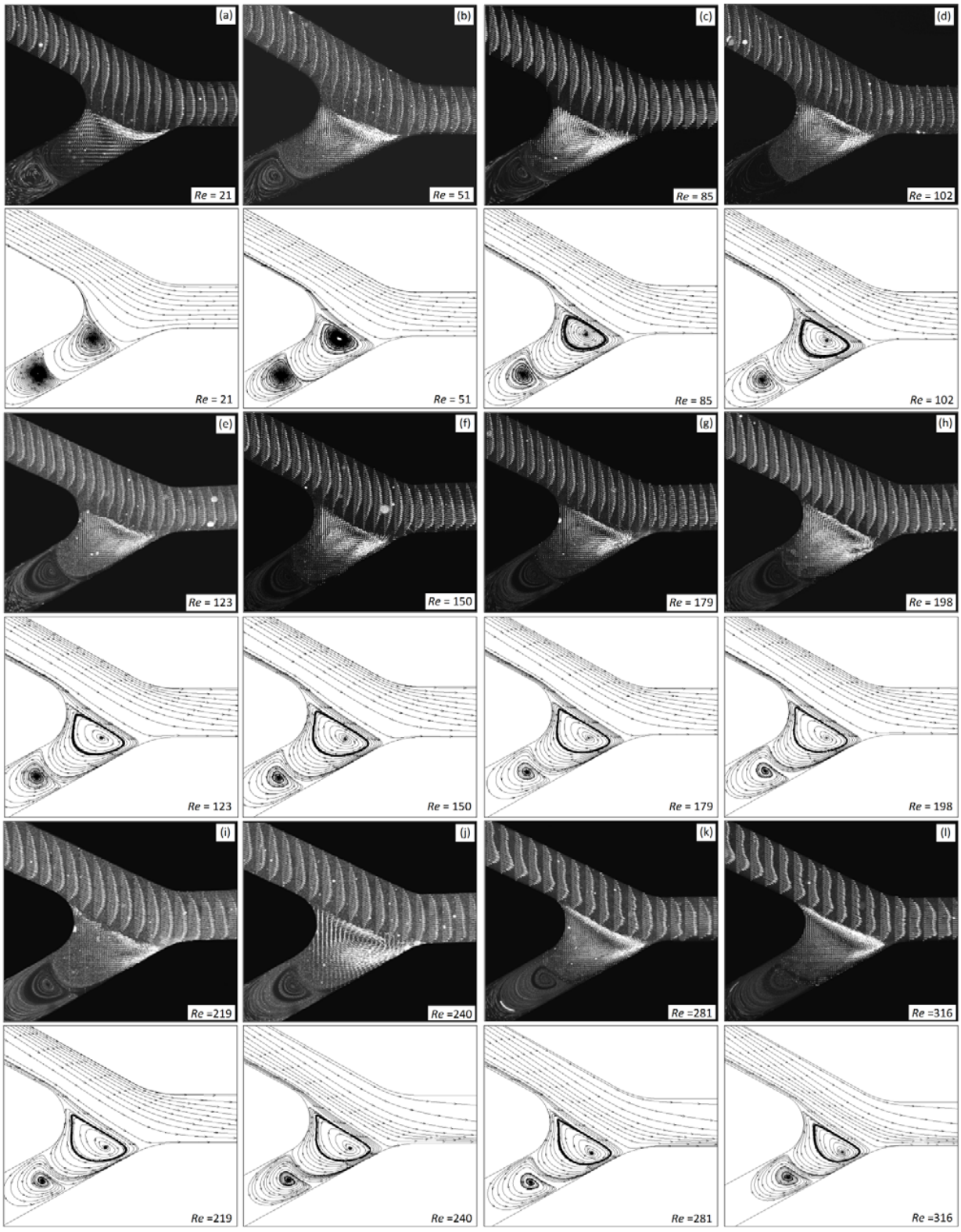

Fig. 5 Qualitative comparison of the microfluidic flow in the Y-bifurcation with one of the branches maintained closed. The Micro-PIV representation of the velocity profiles obtained are made in the median plane of the geometry (flow regime correspond to 21 <*Re*< 316). The first vortex of the secondary flow, developed in the closed branch, is obtained with the Micro-PIV method, with a Δt between images longer then for the corresponding main flows. The second vortex is obtained experimentally by a superposition of several images (70 images)

First we can observe the evolution of the secondary flows manifested in the closed branch of the bifurcation. In this case the secondary flows are manifesting in the form of spiraling vortices, with path lines entering from the middle of the microchannel (median plane region) and exiting above and below near the walls (a numerical representation of the phenomena is given in Fig. 4 (c). The associated geometric parameters that can characterize a vortex structure (e.g. vortex center, stagnation point or separation line between the main and secondary flow) are obtained and put in evidence by pathlines visualizations and velocity measurements.

An important observation has to be made on the vortices from the closed branches, which are developing a movement towards the main flow with the increase of flow rate (Fig. 5 (a) - l). This effect of Newtonian flows is discussed and compared with the opposed behavior of a weekly-elastic fluid flows by Balan et al. [11], but in a slightly different geometry and flow conditions.

The second manifestation observable in this experiment is made on the evolution of velocity profiles in the main flow domain. For a tracking evolution of the velocity in the upstream region of the bifurcation in the open branch at the depth of median plane, the velocity profiles are quantified in the form of graphical representations. This is done from both experimental and numerical point of views, in the range of flow rates that corresponds to $20 < Re < 320$. It is obvious that the velocity profiles are developing asymmetric profiles with the increase of the flow rate (Fig. 4 (d) and (e). This manifestation appears due to the inertial effect amplifications caused by the 60^o deviation of the main flow path before entering in the bifurcation area (Fig. 4 (b). Because of this deviation and due to the increase of flow rate, the Dean vortices – another type of secondary flows - are appearing (numerical representations are given in Fig. 4 (a)). In Fig. 4 (d) and (e) the graphical representations of the velocity profiles are showing also the dependence on *De*. A direct observation is made on how the symmetry of velocity profiles, with respect to the centerline of the channel, is lost for $De > 50$, (the velocity maximum is obtained near the outer wall – Fig. 4 (d) and (e)). This case study is also evidencing the separation between critical microfluidic two-dimensional flows in curved microchannels at lower *De*, from three-dimensional flows that exhibit transverse counter rotating vortices (Dean vortices) at higher *De*. Our onset of Dean vortices in microfluidics is coming from the primary importance in connection with mixing, heat transfer and with a possible transition to a turbulent regime for flows in curved microchannels. A very good agreement between the velocity profiles obtained experimentally and numerically is obtained, with some exceptions near the wall where the resolution and the precision of the Micro-PIV measurements reach the limits of this technique.

B. Measurement Validation on the Case with Bough Branches Open

In the second studied case, the investigations were conducted for a complex hydrodynamic characterization over flow conditions that involved both branches of the Y bifurcation open. Experimental measurements and numerical predictions have been made for a velocity profile determination in the confluence region of the Y geometry, as well as on the common exit up to a distance of 2600 μm from the bifurcation.

Both experimental measurements and numerical predictions reveal two hydrodynamic characteristics of the studied microfluidic flow. The first one is referring to the evolution and the development of secondary flows manifested as symmetrical spiraling vortices. The second one is referring to the stabilization distance for the velocity profiles on the common exit of the flow.

For this flow configuration the hydrodynamic behavior is different when we refer to the secondary flows manifestations. Secondary flows are appearing here for flow regimes with $Re \geq 80$ (Fig. 6) and are manifested as two symmetrical spiraling vortices found in the confluence zone. This qualitative characterization was achieved from both the experimental and the numerical approach, and the results are very similar. From experimental visualizations we have observed that for some of the flow regimes the symmetry of these vortices tends to be lost. This phenomenon was just delusive and it was manifested due to some imperfections in the flow domain - impurities accumulated in one of the inflows. This is the case of flow regime $Re = 160$ (Fig. 9 (a)), were the velocity profiles from each branch are not symmetrical, but when the investigations were performed again the symmetry was present. For the all of the experimental investigations the configuration of the secondary flows were found to be symmetrical and with an increase over the area were this are appearing - very similar with numerical predictions.

A quantitative evolution over the velocity profiles in the confluence zone and in the common exit of the geometry is made in the graphical representations of the Figs. 7, 8 and 9. The experiments performed in this flow case shows a stabilization distance of the velocity profiles smaller than 2500 μm for the flow regimes were $Re \leq 62$ (results presented in Fig. 7), and a stabilization distance that extends far beyond the range of 3000 μm, for the cases with flow regimes characterized by $Re > 70$ (phenomena best seen in the representations from Fig. 9).

V. Conclusions

The main two purposes of this paper were: (i) to identify and analyze the secondary flow manifestations and (ii) to assess the evolution and the manifestation of velocity profiles, visualized and measured, respectively, in two different flow configurations of the same Y bifurcation.

Both developed applications can be seen as benchmark problems for the CFD method (direct comparison of numeric with experiment results) for the investigation the microfluidic problems that involve enhancement of mixing and mass transfer. The dynamics of the vortex formations as secondary flows was characterized relatively to the increase of flow rate for different flow boundary conditions.

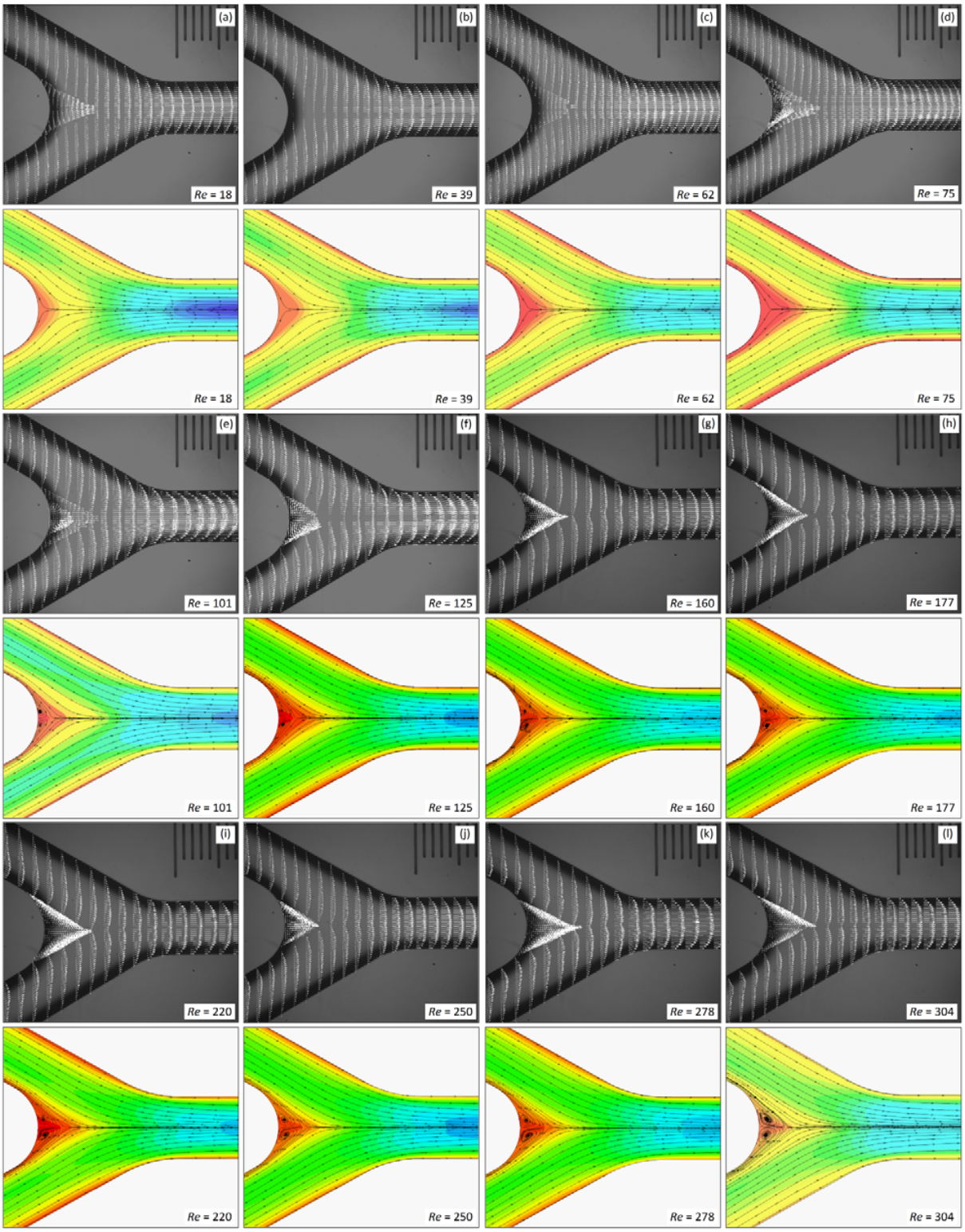

Fig. 6 Qualitative comparison of the microfluidic flows in the Y-bifurcation with both branches open. The Micro-PIV representation of the velocity profiles obtained are made in the median plane of the geometry (flow regime correspond to $18<Re<304$). The secondary flows (manifested as two symmetrical vortex formations) appear for flow regimes with $Re>100$. The numerical predictions represent the path line distribution overlaid on the velocity magnitude mapping.

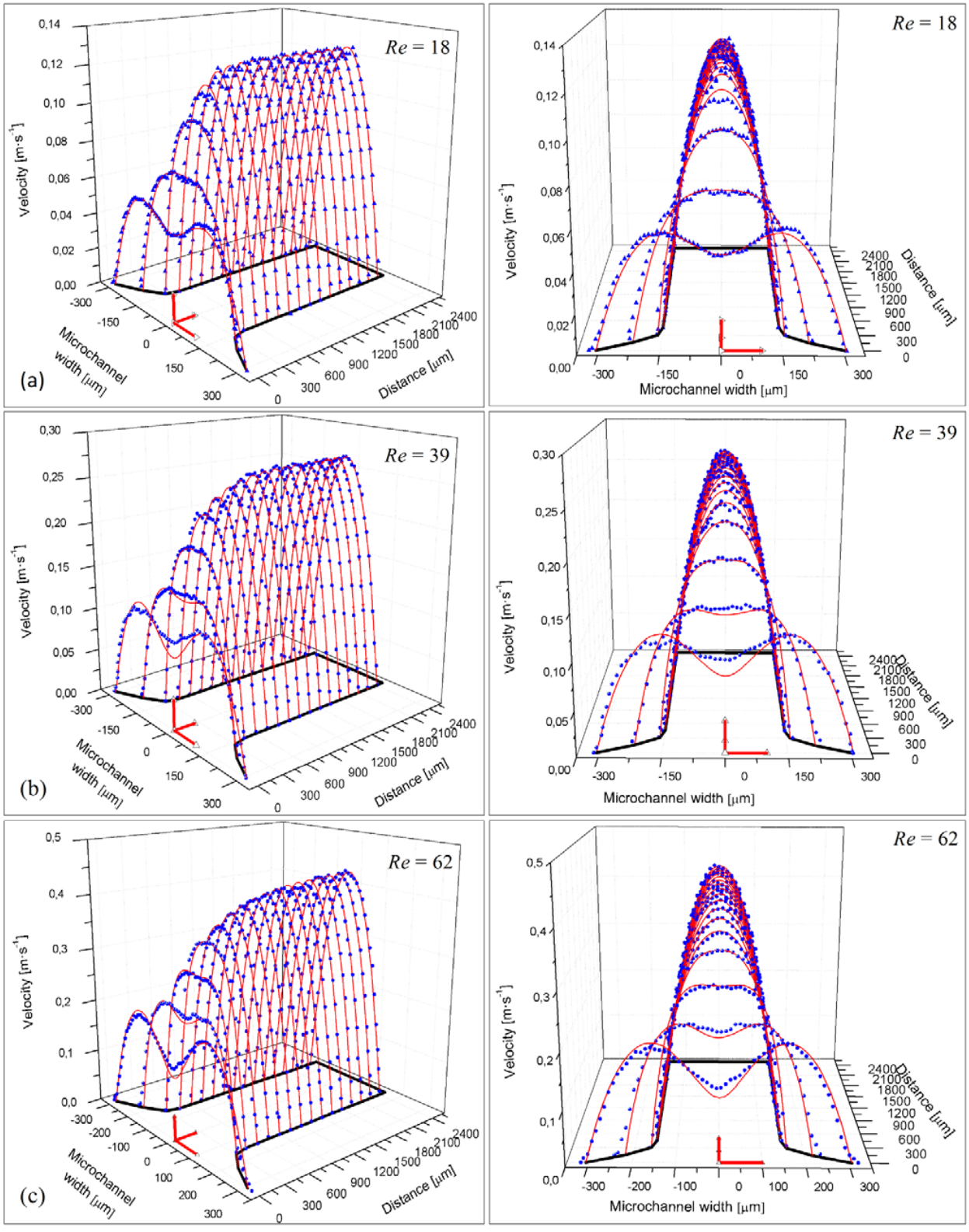

Fig.7 Quantitative comparison of the velocity profiles in the Y-bifurcation with the both branches open. The Micro-PIV representation of the velocity profiles are made in the median plane of the geometry and are compared with the numerical prediction. The evolution of the velocity profiles and the distance stabilization for the flow regimes: (a) *Re* = 18, (b) *Re* = 39, and (c) *Re* = 62

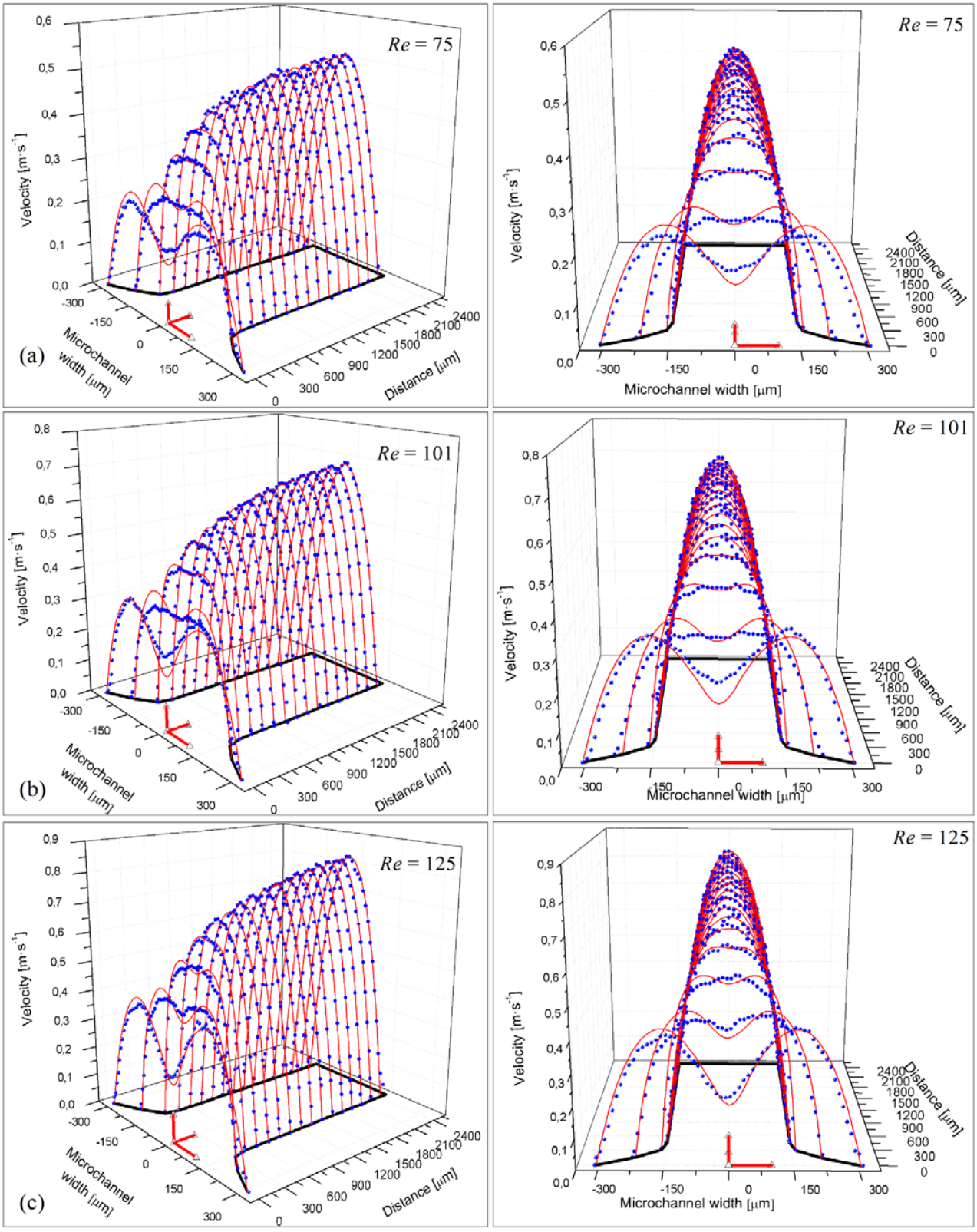

Fig. 8 Quantitative comparison of the velocity profiles in the Y-bifurcation with the both branches open. The Micro-PIV representation of the velocity profiles are made in the median plane of the geometry and are compared with the numerical prediction. The evolution of the velocity profiles and the distance stabilization for the flow regimes: (a) *Re* = 75, (b) *Re* = 101, and (c) *Re* = 125

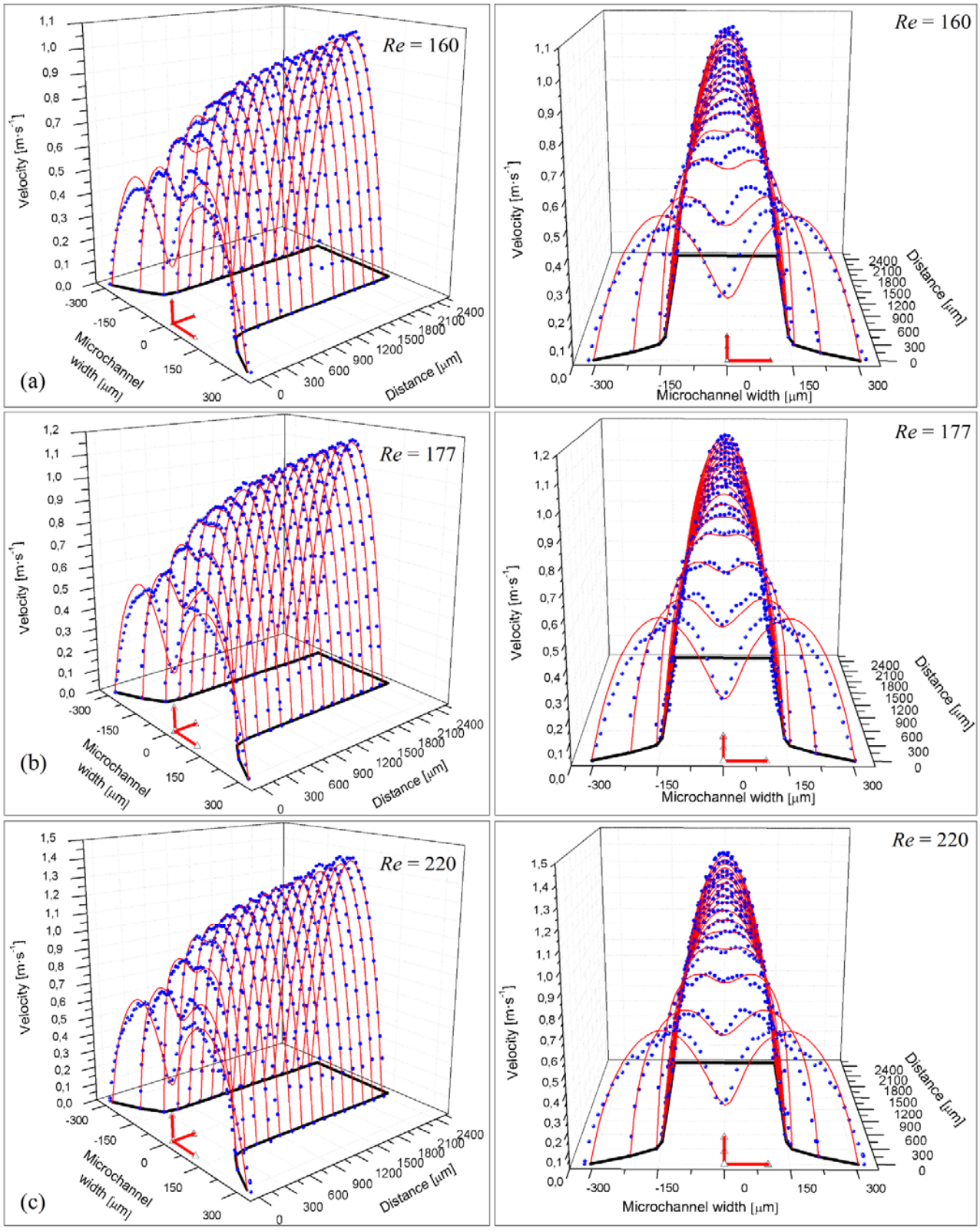

Fig. 9 Quantitative comparison of the velocity profiles in the Y-bifurcation with the both branches open. The Micro-PIV representation of the velocity profiles are made in the median plane of the geometry and are compared with the numerical prediction. The evolution of the velocity profiles and the distance stabilization for the flow regimes: (a) *Re* = 160, (b) *Re* = 177, and (c) *Re* = 220

The direct comparison of flow visualizations with numerical predictions proves that the for the tested microfluidic chips the flows have a pronounced 3D structure.

The conducted experiments confirmed that inertia ($Re \rightarrow \infty$) have a direct impact on the flow pattern. In the first studied case the vortices from the closed branch ware shifted toward the main flow pathlines and Dean vortices are manifesting in the elbow of the geometry with a direct impact on the velocity profiles from the main flow domain. In the second flow conditions the stabilization distance for the velocity profiles ware quantified with Micro-PIV measurements and compared with numerical predictions conducted in the same flow configurations as the experimental ones.

All of the experimental investigations have been performed on microfluidic devices fabricated in silicon wafers. The technique is relatively more expensive and time consuming than PDMS for example, but it results in a more robust architecture that can withstand higher pumping pressures. This technique is better suited for fluids with a high viscosity or for achieving flow regimes that can introduce hydrodynamic instabilities into the bulk flow.

Similar hydrodynamic responses have been observed from both approaches concluding the efficiency and necessity of numerical predictions on designing of microfluidic devices.

ACKNOWLEDGMENT

The authors acknowledge the financial support of the Project *Microfluidic factory for Assisted Self-Assembly of Nanosystems* No. 209, ID 665, funded by the SOP-IEC, O.2.1.2, from which all the infrastructure employed in this paper was purchased.

REFERENCES

[1] H. A. Stone, A. D. Stroock, A. Ajdari, "Engineering flows in small devices: microfluidics toward a Lab-on-a-chip", J. Annu Rev. Fluid Mech. Vol. 36, 2004, pp. 381-411.
[2] C. X. Zhao, A. P. J.Middelberg, "Two-phase microfluidic flows", J. Chemichal Eng. Sci., Vol. 66, 2011, pp. 1394-1411.
[3] S. T. Wereley, C. D. Meinhart, "Recent advances in Micro-Particle Image Velocimetry", Annu. Rev. Fluid Mech., Vol. 42, 2010, pp. 557-576.
[4] S. T. Wereley, C. D. Meinhart, *Micron-resolution particle image velocimetry*, In: Breuer KS (ed) Microscale diagnostic techniques, Springer, Berlin, 2004.
[5] C. D. Meinhart, S. T. Wereley, M. H. B. Gray, "Volume illumination for two-dimensional particle image velocimetry". MeasSciTechnol, Vol. 11, 2000, pp. 809–814.
[6] M. G.Olsen, R. J. Adrian, "Out-of-focus effects on particle image visibility and correlation in microscopic particle image velocimetry", Exp. Fluids, Vol. 29, 2000, S166–S174.
[7] M. Gad-el-Hak, *the MEMS handbook*. CRC Press, 2002, Boca Raton.
[8] S. Kim, S.J. Lee, "Measurement of Dean flow in a curved micro-tube using micro digital holographic particle tracking velocimetry" Exp Fluids, 2009, Vol. 46, pp. 255-264.
[9] S.S. Kuntaegowdanahalli, A.A.S. Bhagat, G. Kumar, I. Papautsky, "Inertial microfluidics for continuous particle separation in spiral microchannels" Lab on a Chip, 2009, Vol. 9, pp. 2973-2980.
[10] A.A.S. Bhagat, S.S. Kuntaegowdanahalli, I. Papautsky, "Continuous particle separation in spatial microchannels using dean flows and different migration" Lab on a Chip, 2008, Vol. 8, pp. 1906-1914.
[11] C. M. Balan, D. Broboana, C. Balan, "Investigation of vortex formation in microbifurcations" Microfluid Nanofluid, 2012, doi 10.1007/s 10404-012-1005-8.